

Characteristics analysis of Fano resonances in MIM waveguide coupled to Π -shaped resonator system with nanorod defect

QIQI MENG¹, YIZHAO PAN¹, YUCHANG LI¹, BOYUN WANG², FANG CHEN^{1*}

¹*Institute of Quantum Optics and Information Photonics, School of Physics and Optoelectronic Engineering, Yangtze University, Jingzhou 434023, China*

²*School of Physics and Electronics-informantion Engineering, Hubei Engineering University, Xiaogan 432000, China*

In this paper, triple Fano resonance (FR) is studied in a defect waveguide coupled to Π -shaped resonator structure. The optical response of the Π -shaped resonator and the nanorod defect can be seen as discrete state and continuous state. The interaction between the narrow discrete states and the broad continuous state produces the triple Fano resonance. Results show that the spectral line shapes of the Fano resonances can be independently tuned by the geometrical parameters. The resonant wavelength of the FR peak has a linear relation with the height and length of the Π -shaped resonator. The sensitivity and maximum *FOM* (figure of merit) can be up to $1340\text{nm}/RIU$, and 7817, respectively. For asymmetrical structure design, a sextuple Fano resonance spectrum is observed. The structure may have potential applications in the field of slow light, plasmonic filters, sensors in complicated environments.

(Received September 24, 2022; accepted June 6, 2023)

Keywords: Surface plasmon polariton, MIM waveguide, Fano resonance, FOM, Π -shaped resonator

1. Introduction

Surface plasmon polaritons (SPPs), propagating electromagnetic waves along the surface of metal and dielectric, have attracted numerous attention due to their unique optical properties [1-4]. Since information traffic has become more and more serious and the design of large-capacity and high-speed information processing systems become urgent. SPPs is considered to be the most competitive new generation of the integrated photonic device because of their strong local field enhancement. Therefore, SPPs have been widely used in biochemistry, energy, and information engineering [5-8]. Many plasmonic structures have been proposed and studied, for example, MIM waveguide structure, metal strips structure, metal films and grooves, metal nanoparticle chains and photonic crystals, metamaterial, and metasurface [9-11]. The MIM structure based on SPPs is widely investigated to realize plasmonic sensors, filters, switches, plasmonic modulators, and slow light [12-17].

Fano resonance in waveguide resonator structure is an interference effect caused by a discrete state and a continuous state. Different from Lorentzian symmetric lineshape, Fano resonance exhibit asymmetric and sharp lineshape with strong field confined. Fano resonance is widely used in optical switches, plasmonic modulators, and nanosensors since its high figure of merit and

sensitivity [18-20]. In the past decade, lots of work is done to investigate Fano resonances in metallic nanostructures. For example, metal nanoparticle array structures, split ring structures and nanoshells structure. But these array structures are hard to integrate into chips which limited their application. Therefore, Fano resonance based on resonator coupled waveguide has been investigated theoretically and demonstrated experimentally. It not only has a simple and compact size, but is also convenient to integrate into chips. For example, Chen et al. Investigated and realized tunable Fano resonance based on MIM waveguide with metal nanowall [21]. Lu et al. designed a sensitive structure based on dual-matrix resonator with its maximum FOM up to 500 [22]. Zhang et al. proposed a double Fano resonance based on M-type cavity coupled MIM waveguide structure with a baffle [23]. Very recently, we also reported an electrically tunable Fano resonance in a ring resonator coupled MIM waveguide with a stub resonator [24].

In this manuscript, triple FR is numerically realized in a compact MIM waveguide system, which is composed of a Π -shaped resonator coupled with a nanorod defect. The transmission characteristics are numerically studied by the finite difference-time domain method (FDTD). The location of the resonance peak and the transmittance can be changed by tuning its structure sizes. Furthermore, the FR responses differently to the variations of the parameter

G. The proposed triple FR can be used as an excellent plasmonic sensor, the calculated sensitivity and FOM are up to 1340 nm/RIU and 7817, respectively. The results of this paper may be important in plasmonic sensors with highly sensitive and accurate sensing, especially in complicated environments.

2. Geometry structure and simulation

The designed triple FR structure is schematically shown in Fig. 1, which is composed of a Π -shaped resonator coupled MIM waveguide, and a nanorod-defect.

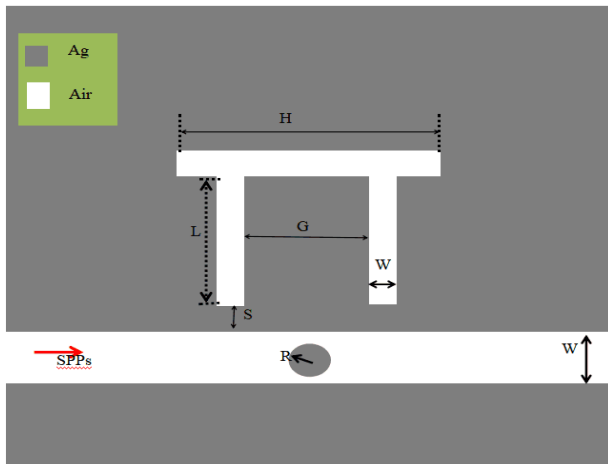


Fig. 1. The schematic diagram of the proposed multiple Fano resonance plasmonic system composed of a defect and a Π -shaped resonator

The parameters used in the paper are as follows: The length and height of Π -shaped resonator are H , L , the defect radius of silver nanorod is R . The distance between the two arms of the Π -shaped resonator is G . The coupling distance between the Π -shaped resonator and the silver nanorod defect is S . It is widely known that silver and gold are the popular materials used in MIM plasmonic waveguide structures, compared with gold, silver has a smaller Drude damping, therefore, in sensing, silver exhibits a higher sensitivity. Furthermore, considering the adhesion between metal and substrate in device manufacturing, silver is also a better material. In sensor components, silver is easily oxidized when exposed to air, which can be solved with a gold veneer that does not oxidize on the surface of the device [25].

In the simulations, the permittivity of silver is characterized by the Drude model:

$$\varepsilon(\omega) = 3.7 - \frac{\omega_p^2}{(\omega^2 + i\omega\gamma_p)} \quad (1)$$

where $\omega_p = 1.37 \times 10^{16} s^{-1}$ is the plasma frequency, and

$\gamma_p = 2.73 \times 10^{13} s^{-1}$ is the damping constant [26], ω is

the angular frequency of the incident light field. Perfect matched layer (PML) is utilized to absorb the outgoing waves. To ensure only the fundamental mode could exist and propagate in the structure, the width of the bus waveguide is set as $w = 50 \text{ nm}$. FDTD solution and Matlab softwares are utilized to calculate the Fano spectra and field patterns. The calculation domain is $2500 \text{ nm} \times 2500 \text{ nm}$, the simulation time is 3000 fs and the rectangular mesh size is $5 \text{ nm} \times 5 \text{ nm}$, perfectly

matched layers (PMLs) are applied in the domain to absorb the input electromagnetic waves. Two power monitors are set at the input and output ports of the bus waveguide to record the electric field and magnetic field.

The transmission is then calculated by the relationship:

$$T = \frac{E_o \times H_o}{E_i \times H_i}$$

where E_o and E_i are the electric field amplitude at the output and input port, H_o and H_i are the magnetic field amplitude at the output and input port.

In the proposed waveguide resonator structure, the phase shift per round trip for the SPPs is expressed as

$$\Delta\varphi = 4\pi n_{eff} L_{eff} / \lambda + 2\varphi \quad [27-28], \quad L_{eff}$$

is the effective length, when the phase shift satisfies the following relationship $\Delta\varphi = 2\pi n$ ($n = 1, 2, 3, \dots$), stable standing wave exists in the resonator, the resonant wavelength is defined as [29]:

$$\lambda = 2n_{eff} L_{eff} (n - \varphi / \pi) \quad (2)$$

where n_{eff} stands for the effective refractive index, it can

be calculated by $n_{eff} = \beta / k_0$. β and k_0 are the phase

propagation constant and wave number of light in free space, φ stands for the phase change brought by the

SPPs reflection in resonator metal wall, n represent the resonant order. The proportionality coefficient is

$$\frac{d\lambda}{dL} = 2n_{eff} \left(n - \frac{\varphi}{\pi} \right) \quad (3)$$

the MICMT theory can be used to study the transmission spectrum. The time evolution amplitude a_n of the

Π -shaped resonator can be described as follows:

$$\frac{da_n}{dt} = (-j\omega_n - \frac{1}{\tau_{n0}} - \frac{1}{\tau_{n1}} - \frac{1}{\tau_{n2}})a_n + k_{n1}S_{n,1+} + k_{n2}S_{n,2+} \quad (4)$$

$$S_{1-} = -S_{1+} + \sum_n k_{n1}^* a_n \quad (5)$$

$$S_{2-} = -S_{2+} + \sum_n k_{n2}^* a_n \quad (6)$$

$$S_{n,1+} = e^{j\varphi_{n1}} S_{1,+} \quad (7)$$

$$S_{n,2+} = e^{j\varphi_{n2}} S_{2,+} \quad (8)$$

where ω_n are the n_{th} resonant frequency, $\tau_{n,i}$ ($i=1,2$)

are the decay time of the coupling between the Π -shaped resonator and the bus waveguide, the coupling coefficient

$k_{n,i}$ ($i=1,2$) of the n_{th} mode can be calculated by :

$$k_{n1} = \sqrt{\frac{2}{\tau_{n1}}} e^{j\theta_{n1}} \quad (9)$$

$$k_{n2} = \sqrt{\frac{2}{\tau_{n,2}}} e^{j(\theta_{n1} - \phi_n)} \quad (10)$$

Here, θ_i ($i=1,2$) are the phase of the coupling coefficient, $\phi_{n,i}$ are the phase change from input to output part of the n_{th} resonant mode. For the proposed configuration,

$$\tau_{n1} = \tau_{n2} = \tau_n \quad (11)$$

and the total coupling phase change of the n_{th} resonant mode can be expressed as

$$\varphi_n = \varphi_{n1} + \phi_n \quad (12)$$

according to MICMT theory [30-31], when $S_{2+} = 0$, the complex amplitude transmission coefficient is given as follows:

$$T = \left| \frac{S_{2-}}{S_{1+}} \right|^2 = \left| \sum_n \frac{2e^{j\varphi_n}}{-j(\omega - \omega_n)\tau_n + 2 + \frac{\tau_n}{\tau_{n0}}} \right|^2 \quad (13)$$

To study the formation principle of the designed Fano resonance structure, transmission spectra are shown in Fig.

2, the geometrical parameters are shown in Table 1. In practical setup, a polychromatic light source is used as light source for their coverage over the range of the resonant wavelength. A single-mode fiber (SMF) carries the light to the input port of the sensor. The output port of the sensor is linked to an optical spectrum analyzer (OSA) through another SMF to detect variations in resonant wavelength [32].

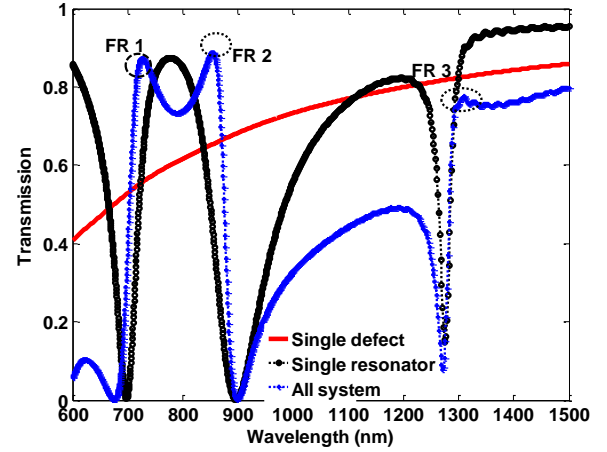


Fig. 2. The transmission spectra of the coupled plasmonic system calculated by FDTD. (The geometrical parameters were set as $w = 50$ nm, $s = 10$ nm, $H = 400$ nm, $L = 215$ nm, $R = 20$ nm, $G = 300$ nm) (color online)

Table 1. The symbol and quantity of the model parameters

Parameter	Symbol	Quantity	Unit
Width of the bus waveguide	w	50	nm
Coupling distance between the Π -shaped resonator and bus waveguide	s	10	nm
Length of the horizontal arm	H	400	nm
Height of the vertical arm	L	215	nm
Radius of the defect	R	20	nm
Distance between the two vertical wall	G	300	nm
Width of the Π -shaped resonator	w	50	nm

When there is only a nanorod defect, a broad continuous spectrum is produced. With only Π -shaped resonator, we can see three resonant modes with small transmittance. For the whole structure, triple FR (labeled by FR1, FR2, FR3) located at $\lambda_1 = 723$ nm, $\lambda_2 = 853$ nm, $\lambda_3 = 1299$ nm. The interference between the broad continuous state and the narrow discrete state leads to the FR. To further study the mechanism of the FR, the

steady-state magnetic field $|H_z|^2$ distributions are calculated. The sign mode (m,n) is utilized to stand for different modes exists in the Π -shaped cavity. The number m and n indicate the antinodes number of standing waves in the x and y directions [33]. It can be noticed in Fig. 3 that the excited resonant modes are mode $(2,1)$, mode $(1,1)$ and mode $(0,1)$, respectively.

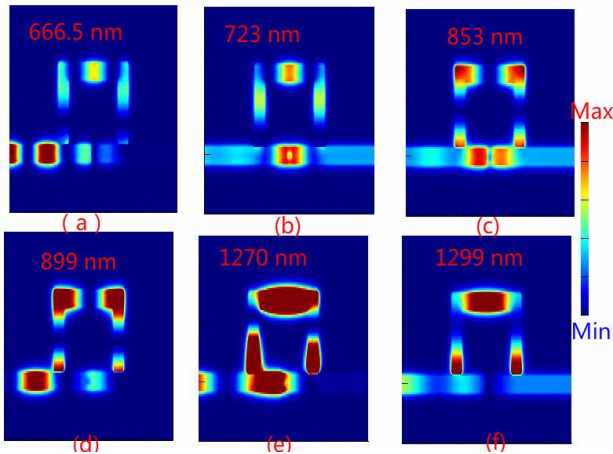
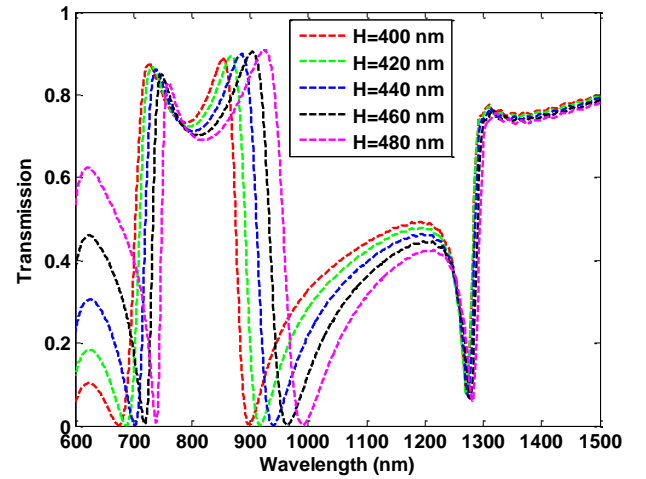
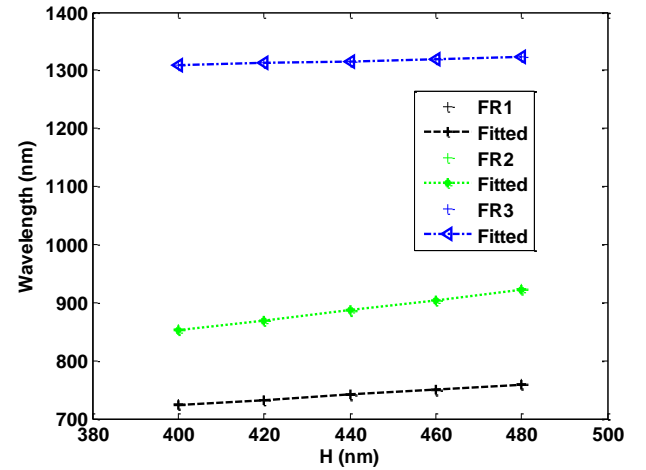


Fig. 3. Contour profiles of the magnetic field $|H_z|^2$ (a) 66.5 nm (b) 723 nm (c) 853 nm. (d) 899 nm (e) 1270 nm (f) 1299 nm (color online)

Fig. 3(a) depicts the field intensity distribution of 666.5 nm (FR1 dip), it can be noticed that the SPPs are coupled into the Π -shaped resonator and then it is reflected back. At FR1 peak 723 nm, the light wave can be coupled into the resonator, and the silver nanorod-defect is then excited and most of the magnetic field is transmitted to the output. At FR2 peak 853 nm, most of the magnetic field is confined in the corners of the Π -shaped resonator and silver nanorod-defect. At FR2 dip 899 nm, the same phenomenon can be observed, but the incident wave and the reflected wave are out-of-phase, and the destructive interference leads to almost zero transmittance. The field distribution in the Π -shaped resonator at the FR3 is displayed in Fig. 3(e) and (f), revealing mode $(0,1)$ is excited in the Π -shaped resonator.



a



b

Fig. 4. (a) The transmission spectra of the plasmonic Fano system with different H . (b) Dependence of the resonant wavelength on the parameter of H (color online)

The influences of Π -shaped resonator's size H on the transmittance are studied. When H increases from 400 nm to 480 nm with fixed $w=50$ nm, $s=10$ nm, $L=215$ nm, $R=20$ nm, $G=300$ nm, as shown in Fig. 4(a), the resonant wavelengths of FR1 and FR3 show a red-shifted. Fig. 4(b) shows the dependence of resonant wavelength on the parameter of H , a linear relationship can be observed (FR1: $\Delta\lambda/\Delta H=0.45$; FR2: $\Delta\lambda/\Delta H=0.88$; FR3: $\Delta\lambda/\Delta H=0.18$). According to the equation 2, the resonant wavelength becomes larger with increasing H .

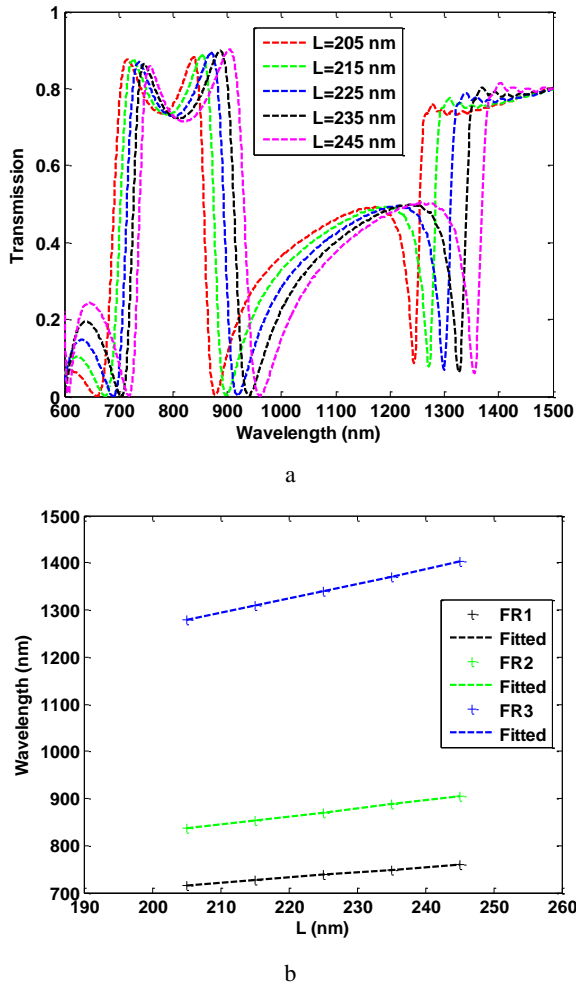


Fig. 5. (a) The transmission spectra of the plasmonic Fano system with different L . (b) Dependence of the resonant wavelength on the parameter of L (color online)

The transmittance spectra with different L are shown in Fig. 5(a), when L increases from 205 nm to 245 nm, the resonant peaks of FR1, FR2 and FR3 show red shift. At the same time, the transmittance nearly keeps unchanged. Fig. 5(b) shows the relationship between the resonant wavelength and L , and there exists a linear relationship (FR1: $\Delta\lambda/\Delta L=1.08$; FR2: $\Delta\lambda/\Delta L=1.65$; FR3: $\Delta\lambda/\Delta L=3.1$). Comparing the sensitivity to the length H and height L of the Π -shaped resonator, the response is quite different, resonant wavelength is more sensitive to the change of height L , it is because the effective resonant length are $4L+H$ and $2L+H$ for mode (2,1) and mode (1,1). Therefore, the FR wavelength can be roughly controlled by tuning the size of L or fine regulation by tuning the size of H .

Fig. 6(a) shows the transmission spectra with different nanorod defect radius R , we can see that the FR peaks are gradually decreased as R increases. It can be analyzed as follows: the transmission spectrum of nanorod defect is continuous, the bigger R lead to lower transmittance, therefore FR peaks are getting smaller. Fig. 6(b) shows the transmittance spectra with different coupling distances s . When s increases from 10 nm 35 nm, it can be noticed that the FR peaks are becoming smaller. This is because a larger coupling distance means less energy can be coupled into the Π -shaped cavity. Therefore, one can control the FR resonance by tuning the distance of coupling distance and the size of the nanorod defect.

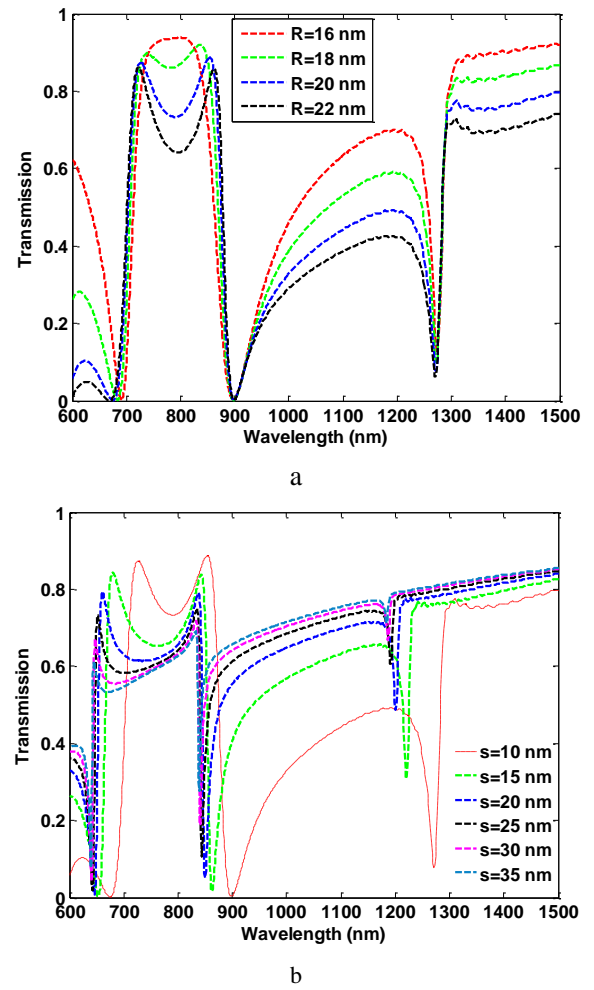


Fig. 6. (a) The transmission spectra of the plasmonic Fano system with different R . (b) The transmission spectra of the plasmonic Fano system with different s (color online)

To study the effect of G on the Fano spectrum, Fig. 7(a) shows the transmission spectra with different G , it can be noticed that the amplitude of FR1 becomes weaker with G decreases, but the amplitude of FR2 and FR3 almost keep unchanged. Fig. 7(b) depicts the magnetic-field distribution $|H_z|^2$ of the plasmonic Fano system with $G=190$ nm. From Fig. 7 (b) and (c) it can

be noticed that at 630 nm, the two vertical arms of the Π -shaped resonator are located at the antinode of the horizontal arm. The mode (2,1) cannot be excited under these circumstances, therefore, FR1 is restrained. While the mode (1,1) and mode (0,1) are hardly affected, only

the position of resonance wavelength is changed, since the coupling between the vertical arm and the bus waveguide is changed with the movement of the vertical arm. Therefore, we can independently tune FR1 by changing the size of G .

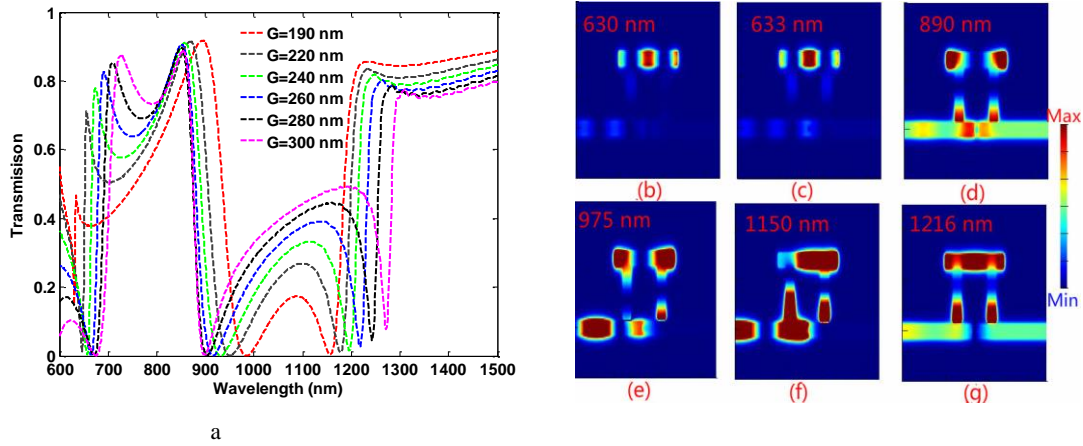


Fig. 7. (a). The transmission spectra of the plasmonic Fano system with different G . (b)-(g) The magnetic field distribution $|H_z|^2$ of the plasmonic Fano system with $G = 190$ nm (color online)

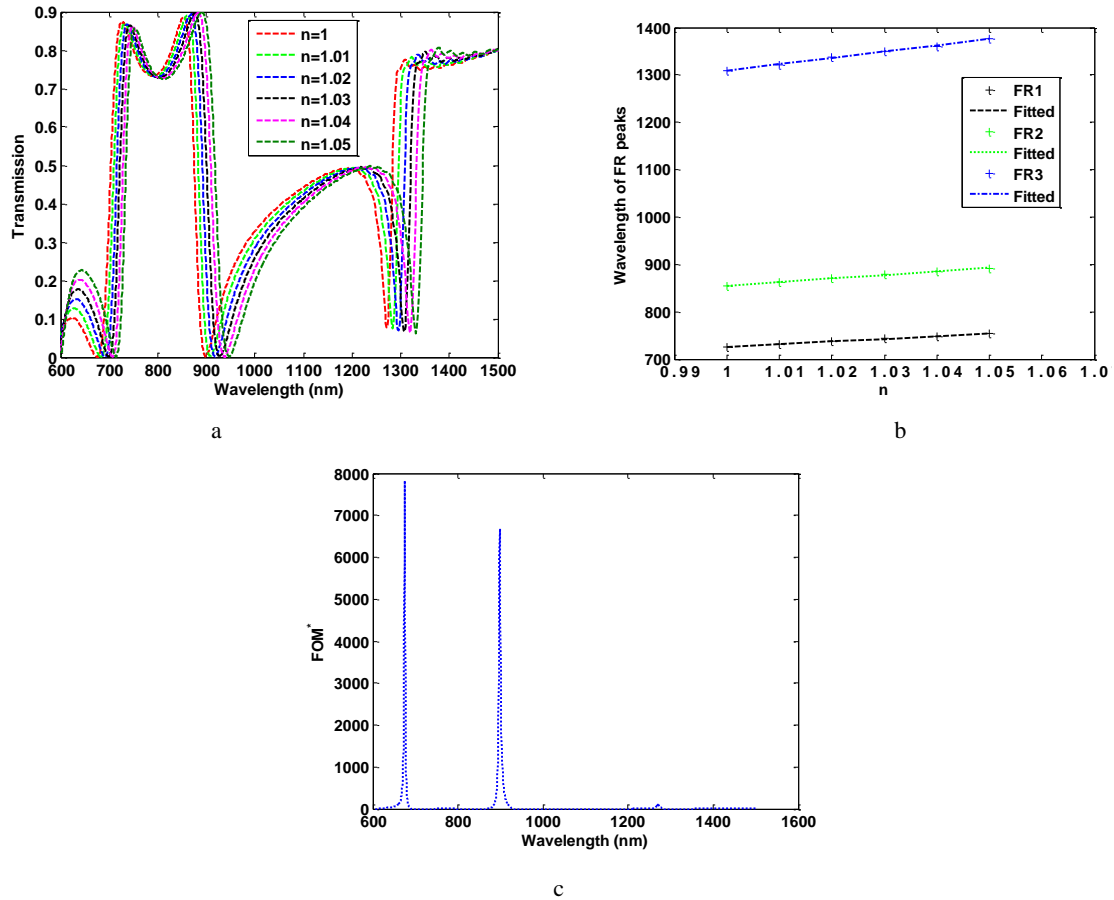


Fig. 8. (a) The transmission spectra of the proposed plasmonic Fano system with changing n from 1.00 to 1.05. (b) The resonant wavelength of FR1, FR2, FR3 with different n . (c) The FOM^* distribution with the wavelength of the structure (color online)

Fig. 8 (a) depicts the relationship between the transmittance spectra and refractive index n . One can see that when n increases from 1 to 1.01, 1.02, 1.103, 1.04 and 1.05, the FR peaks show redshift. To better evaluate the sensing performance, the sensitivity is calculated with $w = 50 \text{ nm}$, $s = 10 \text{ nm}$, $H = 400 \text{ nm}$, $L = 215 \text{ nm}$, $R = 20 \text{ nm}$, $G = 300 \text{ nm}$. According to the paper [36], refractive index sensitivity is defined by:

$$S = d\lambda / dn \text{ (nm/RIU)} \quad (14)$$

From Fig. 8(b) it can be noticed that the relationship between resonant wavelength and the refractive index is linear, the sensitivity is about 600 nm/RIU, 760 nm/RIU, and 1340 nm/RIU at FR1, FR2, and FR3, respectively. The sensing performance of other related works is compared and the results are shown in Table 2.

Table 2. Sensing comparisons between the proposed structure and other works

References	Year	Structure	Sensitivity
This work	2022	II-shaped resonator with defect	1340 (nm/RIU)
R35	2021	Equilateral triangular resonator	923 (nm/RIU)
R36	2020	Double split ring resonator	1260(nm/RIU)
R37	2018	Two metallic SRRS and a nanorod	552(nm/RIU)
R38	2013	3D nanorod metasurface	1250(nm/RIU)
R39	2019	Circular arrays of nanorods and nanotubes	1055(nm/RIU)
R40	2020	Dual side coupled rectangular resonators	1090(nm/RIU)
R41	2021	Waveguide coupled with square ring resonator	1074.8(nm/RIU)
R42	2021	Waveguide coupled resonator with defects	25.4(nm/MPa)
R43	2022	Waveguide coupled with concentric ring resonator	3639(nm/RIU)
R44	2021	Cog-shaped resonator with waveguide	6227(nm/RIU)
R45	2021	Waveguide with multiple ring resonators	3573(nm/RIU))

The sensitivity of the present structure is relatively good compared to previous work [35-45]. In practical sensing applications, a high FOM is required. $FOM = \Delta T(\lambda) / T(\lambda) \Delta n(\lambda)$, where $\Delta T(\lambda) / \Delta n(\lambda)$ stands for the transmittance variation due to the change of the refractive index and $T(\lambda)$ denotes the transmittance of a specific wavelength.

The FOM value in the proposed structure is calculated, as shown in Fig. 8(c), the maximum FOM is up to 7817. Compared to other related work, the FOM of the proposed structure is relatively better [46].

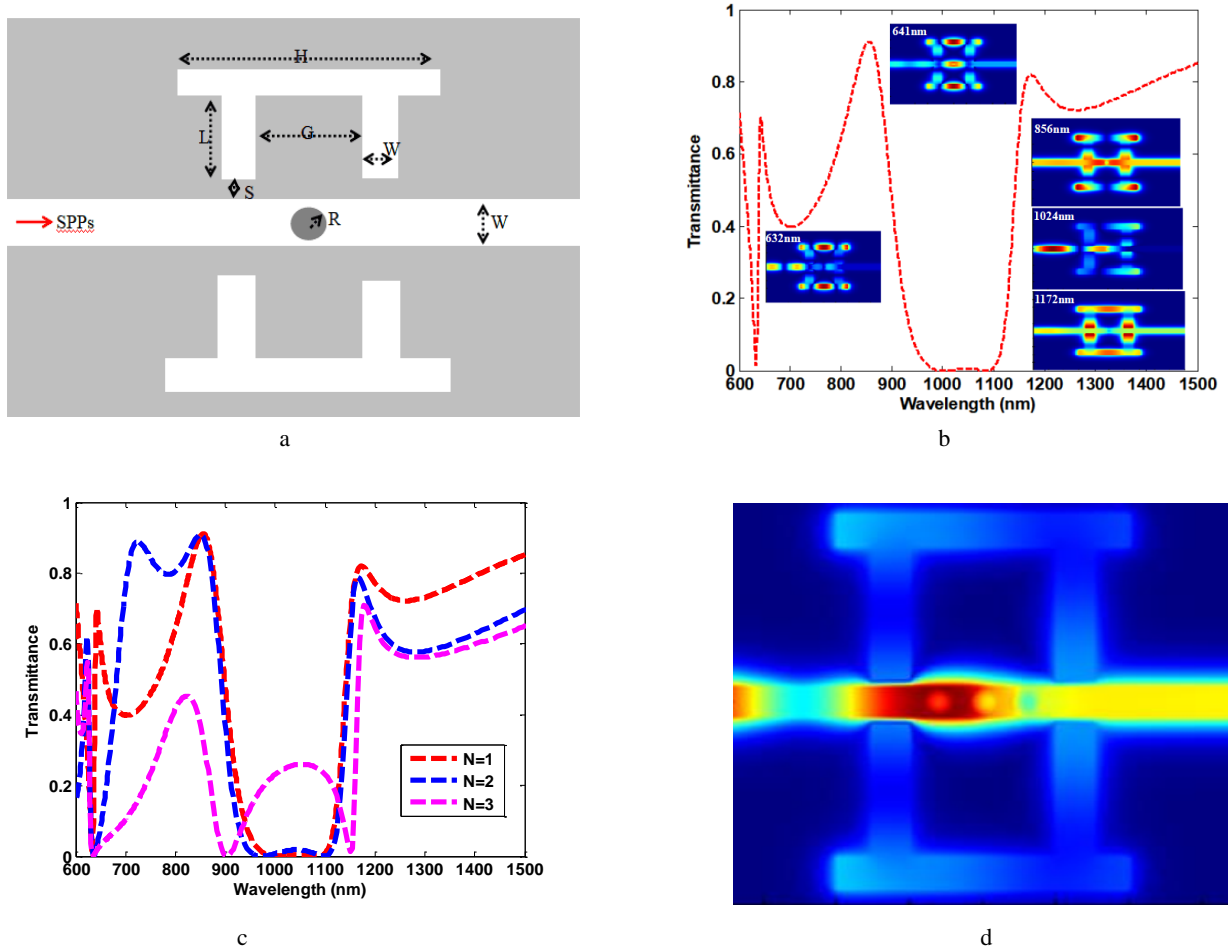


Fig. 9. (a) The schematic diagram of the symmetrical Π -shaped resonator system. (b) The transmission spectra of the symmetrical system, the inset is the magnetic field $|H_z|$. (c) The transmission spectra with different numbers of defect in the bus waveguide. (d) Gap plasmonic resonances (color online)

Another Π -shaped resonator is added at the other side of the bus waveguide to form a symmetrical structure, as shown in Fig. 9(a). The parameters are set as follows: $w = 50 \text{ nm}$, $s = 10 \text{ nm}$, $H = 400 \text{ nm}$, $L = 215 \text{ nm}$, $R = 20 \text{ nm}$, $G = 200 \text{ nm}$. Using the FDTD method to simulate the structure, the transmission spectrum is shown in Fig. 9(b). It can be seen that three sharp asymmetric Fano resonances occur when the resonant wavelengths are 641 nm, 856 nm, and 1172 nm, respectively. The inset of Fig. 9 is the magnetic field $|H_z|^2$.

Fig. 9 (c) shows the transmission spectra with different numbers of defect in the bus waveguide. For FR3, we can see the transmittance of the FR peak is decreased with increasing the number of defect. The anti-symmetric curve becomes steeper (the distance between the Fano peak and Fano dip reduces from 84 nm to 32 nm), which is benefit to the sensitivity, this is because the strong coupling of light within the *gaps between nanorod defect*. Fig. 9 (d) shows the magnetic field when there are three defects in the bus waveguide, the field pattern can verify the gap plasmonic resonance [47].

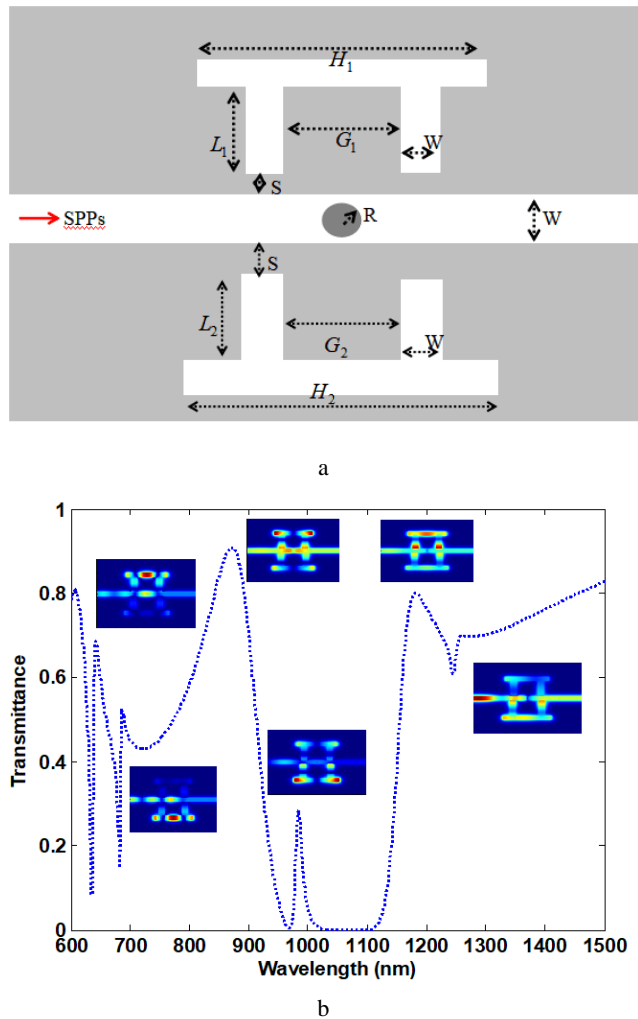


Fig. 10. (a) The schematic diagram of the asymmetrical Π -shaped resonator system. (b) The transmission spectra of the asymmetrical system, the inset is the magnetic field. The geometrical parameters were set as $w = 50 \text{ nm}$, $s = 10 \text{ nm}$, $H_1 = 400 \text{ nm}$, $L_1 = 215 \text{ nm}$, $R = 20 \text{ nm}$, $G_1 = 200 \text{ nm}$, $H_2 = 440 \text{ nm}$, $L_2 = 215 \text{ nm}$, $G_2 = 220 \text{ nm}$ (color online)

By changing the sizes of the lower Π -shaped resonator, asymmetrical configuration can be introduced, Fig. 10(b) depicts six Fano resonance peaks in the transmission spectrum. The corresponding magnetic field $|H_z|$ distributions of the Fano peaks are also shown. The number of Fano resonances of the asymmetrical structure is significantly more than the symmetric structure. Therefore, we can design a multi-wavelength Fano resonance sensor based on the proposed asymmetrical structure.

3. Conclusion

In conclusion, triple FR has been investigated based on MIM waveguide coupled Π -shaped resonator with a nanorod defect. The results indicate that asymmetric FR can be controlled by tuning the geometrical sizes, such as the length of Π -shaped resonator, and the radius of nanorod-defect. The FR1 can be changed independently by tuning the distance of the arms of the Π -shaped resonator. Due to the ultra-sharp line shape, a figure of merit of about 7817 and a sensitivity of about 1340 nm/RIU were obtained. A sextuple Fano resonance spectrum is observed with an asymmetrical structure design. The proposed triple FR structure has important applications in sensing since its high refractive index sensitivity and good FOM.

Acknowledgement

Supported by the National Natural Science Foundation of China (Grant No. 11747091), and the Natural Science Foundation of Hubei Province, China (Grant No 2022CFB475).

References

- [1] J. Tao, X. G. Huang, X. S. Lin, Q. Zhang, X. P. Pin, Optics Express **17**, 13989 (2009).
- [2] F. Ling, Z. Q. Zhong, R. S. Huang, B. Zhang, Sci. Rep. **8**, 9843 (2018).
- [3] F. Chen, H. F. Zhang, L. H. Sun, J. J. Li, C. C. Yu, Opt. Laser. Technol. **116**, 293 (2019).
- [4] T. J. Yen, W. J. Padilla, N. Fang, D. C. Vier, D. R. Smith, J. B. Pendry, D. N. Vasov, X. Zhang, Science **303**, 1494 (2004).
- [5] L. Xie, W. Gao, J. Shu, Y. Ying, J. Kono, Sci. Rep. **5**, 8671 (2015).
- [6] D. Dutta-Gupta, O. J. F. Martin, S. D. Gupta, G. S. Agarwal, Optics Express **20**(2), 1330 (2012).
- [7] S. Kim, J. Jin, Y.-J. Kim, I. -Y. Park, Y. Kim, S. -W. Kim, Nature **453**(7196), 757 (2008).
- [8] D. N. Jones, N. Liu, B. Cortbett, P. Lovera, A. J. Quinn, A. O'Riordan, J. Phys. Conf. Ser. **307**, 012005 (2011).
- [9] L. V. Brown, H. Sobhani, J. B. Lassiter, P. Nordlander, N. J. Halas, ACS Nano **4**, 819 (2010).
- [10] S. L. Li, Y. L. Wang, R. Z. Jiao, L. L. Wang, G. Y. Duan, L. Yu, Optics Express **25**, 3525 (2017).
- [11] A. D. Khan, G. Miano, Plasmonics **8**, 1429 (2013).
- [12] X. Ren, K. Ren, Y. Cai, Appl. Opt. **56**, 11 (2017).
- [13] J. Chen, C. Sun, Q. Gong, Opt. Lett. **39**, 52 (2014).
- [14] K. Wen, Y. Hu, L. Chen, J. Zhou, M. He, L. Lei, Z.

- Meng, *IEEE Photonics J.* **7**, 4801807 (2015).
- [15] Z. Zhang, J. Wang, Y. Zhao, D. Lu, Z. Xiong, *Plasmonics* **6**, 773 (2011).
- [16] T. Nurmohammadi, K. Abbasian, R. Yadipour, *Opt. Commun.* **410**, 142 (2018).
- [17] N. Jankovic, N. Cselyuska, *Sensors* **18**, 287 (2018).
- [18] F. Chen, H. F. Zhang, L. H. Sun, C. C. Yu, *Optik*, **212**, 164755 (2020).
- [19] F. Chen, H. F. Zhang, L. H. Sun, J. J. Li, C. C. Yu, *Optik*, **185**, 585 (2019).
- [20] Y. Wang, S. Li, Y. Zhang, L. Yu, *IEEE Photonics J.* **8**, 1 (2016).
- [21] J. Qi, Z. Chen, J. Chen, Y. Li, W. Qiang, J. Xu, Q. Sun, *Opt. Express* **22**, 14688 (2014).
- [22] H. Lu, X. Liu, D. Mao, G. Wang, *Opt. Lett.* **37**, 3780 (2012).
- [23] L. T. Qiao, G. M. Zhang, Z. S. Wang, G. P. Fan, Y. F. Yan, *Opt. Commun.* **433**, 144 (2019).
- [24] F. Chen, D. Z. Yao, *Opt. Commun.* **369**, 72 (2016).
- [25] R. Malureanu, A. Lavrinenko, *Nanotechnol. Rev.* **4**, 259 (2015).
- [26] B. F. Yun, R. H. Zhang, G. H. Hu, Y. P. Cui, *Plasmonics* **11**, 1157 (2016).
- [27] J. J. Chen, Z. Li, S. Yue, J. H. Xiao, Q. H. Gong, *Nano Lett.* **12**, 2494 (2012).
- [28] F. F. Hu, H. X. Yi, Z. P. Zhou, *Opt. Lett.* **36**, 1500 (2011).
- [29] S. L. Li, Y. L. Wang, R. Z. Jiao, L. L. Wang, G. Y. Duan, L. Yu, *Opt. Express* **25**, 3525 (2017).
- [30] S. Wang, S. L. Yu, T. G. Zhao, Y. S. Wang, X. T. Shi, *Opt. Commun.* **465**, 125614 (2020).
- [31] S. L. Li, Y. Y. Zhang, X. K. Song, Y. L. Wang, L. Yu, *Optics Express* **24**, 15351 (2016).
- [32] M. F. Hassan, R. H. Sagor, M. R. Amin, M. R. Islam, M. S. Alam, *IEEE Sens. J.* **21**, 17749 (2021).
- [33] P. Berini, *Optics Express* **14**, 13030 (2006).
- [34] K. Wen, Y. Hu, L. Chen, J. Zhou, L. Lei, Z. Meng, *Plasmonics* **11**, 315 (2015).
- [35] G. L. Xiao, Y. P. Xu, H. Y. Yang, Z. T. Ou, J. Y. Chen, H. O. Li, X. P. Liu, L. Z. Zeng, J. Q. Li, *Sensors* **21**, 1164 (2021).
- [36] G. L. Lan, Z. X. Jin, J. P. Nong, P. Luo, C. C. Guo, Z. G. Sang, L. Dong, W. Wei, *Appl. Sci.* **10**, 2295 (2020).
- [37] Y. L. Wang, S. L. Li, Y. Y. Zhang, L. Yu, *Plasmonic* **13**, 107 (2018).
- [38] H. Q. Wang, C. Z. Fan, J. N. He, P. Ding, E. J. Liang, Q. Z. Xue, *Optics Express* **21**, 2236 (2013).
- [39] M. R. Rakhshani, *J. Opt. Soc. Am. B* **36**, 2834 (2019).
- [40] M. R. Rakhshani, *Photonic Nanostruct.* **39**, 100768 (2020).
- [41] I. Tathfif, K. S. Rashid, A. A. Yaseer, R. H. Sagor, *Result in Physics* **29**, 104795 (2021).
- [42] I. Tathfif, A. A. Yaseer, R. H. Sagor, K. S. Rashid, *Optics Express* **29**(20), 32365 (2021).
- [43] A. A. Yaseer, I. Tathfif, M. F. Hassan, K. S. Rashid, R. H. Sagor, *Opt. Commun.* **519**, 128429 (2022).
- [44] K. S. Rashid, I. Tathfif, A. A. Yaseer, M. F. Hassan, *Optics Express* **29**(23), 37541 (2021).
- [45] K. S. Rashid, M. F. Hassan, A. A. Yaseer, I. Tathfif, R. H. Sagor, *Sensing and Bio-Sensing Research* **33**, 100440 (2021).
- [46] R. E. Haffar, A. Farkhsi, O. Mahboub, *Appl. Phys. A* **126**, 486 (2020).
- [47] P. Ji, Q. H. Shi, L. Zheng, G. H. Wang, F. Chen, *Optical and Quantum Electronics* **54**(3), 184 (2022).

*Corresponding author: chenfang@yangtzeu.edu.cn